4-2023

Nanostructure Scaling in Semi-Dilute Triblock Copolymer Gels

Kenny Mineart
Bucknell University, kpm007@bucknell.edu

Matthew J. Vallely
Bucknell University

Emma K. O'Shea
Bucknell University

Nanostructure Scaling in Semi-Dilute Triblock Copolymer Gels

Kenneth P. Mineart, Matthew J. Vallely, Emma K. O'Shea*

K. P. Mineart, M. J. Vallely
Department of Chemical Engineering, Bucknell University, Lewisburg, PA 17837, USA
E-mail: kpm007@bucknell.edu

E. K. O'Shea
Department of Biomedical Engineering, Bucknell University, Lewisburg, PA 17837, USA

Keywords: block copolymer, polymer gel, SAXS, scaling theory

There is a considerable body of work that describes the scaling of diblock copolymer micelle dimensions in dilute and semi-dilute solution based upon block degrees of polymerization and copolymer concentration. However, there is a lack of analogous information for semi-dilute ABA triblock copolymer gels, which consist of ABA triblock copolymer dissolved in midblock-selective (B-selective) solvent. The present study uses small angle x-ray scattering to extract micelle dimensions for numerous triblock copolymer gels that vary in copolymer identity (and hence block lengths) and copolymer concentration, as well as gels that contain various ratios of two unique triblock copolymers. Analysis of micelle structural data subsequently translates to universal scaling expressions for the micelle core radius – $r_A \sim N_A^{0.53} N_B^{-0.14} \phi_{ABA}^{0.16}$ where N_A and N_B are the endblock and midblock degrees of polymerization, respectively, and ϕ_{ABA} is the volume fraction of triblock copolymer in the gel – and for the intermicelle spacing – $l_{AA} \sim N_A^{0.09} N_B^{0.29} \phi_{ABA}^{-0.35}$. Each scaling expression describes the full collection of experimental data very well. Additionally, these scaling expressions are partially in line with expectations from semi-dilute diblock copolymer solution theory.

1. Introduction

The nanoscale structure of block copolymer solutions is a topic that has sustained interest for some time beginning with exploration of the factors that affect diblock copolymer micelle dimensions in dilute solutions ($\phi < \phi^*$ where ϕ and ϕ^* are the copolymer volume fraction and the overlap volume fraction, respectively).[1] This area has greatly expanded to include, among other things, the development of detailed phase diagrams in mixtures of block copolymers with solvents of varying selectivity.[2,3] Scaling analysis within the former was initiated by work of de Gennes[4] who extended theory of polymer brushes at planar interfaces to the micellar geometry (**Figure 1a**). In particular, de Gennes found that, in the limit of relatively short solvophilic blocks (*i.e.*, crew-cut micelles), the micelle core radius – r_A – should scale with $N_A^{2/3}$ where N_A is the solvophobic block's degree of polymerization. Zhulina and Birshtein[5] expanded upon this work by considering a broad range of copolymer micelle core-corona asymmetries. They concluded that the scaling of structural features changes depending on copolymer composition (and consequently micelle asymmetry) and describe composition regimes from low solvophilic block fraction (crew-cut micelles) to high solvophilic block fraction (small micelles with long coronal chains). Their theory corroborates that of de Gennes for crew-cut micelles, as well as, establishes several additional predictions including that r_A has dual dependence on N_A and N_B – the solvophilic block's degree of polymerization – for hairy micelles (*i.e.*, those formed by diblock copolymers with $N_A^{0.62} < N_B < N_A^{0.74}$ in good solvent). Their work also provides expectations for the scaling behavior of corona thickness – l_B – (**Figure 1a**) in each identified composition regime. Alternative theoretical frameworks have been used to model dilute diblock copolymer micelles and their results mostly align with those described above.[6,7]

Theories for dilute solutions make scaling predictions based on the free energy of an isolated micelle. In many cases, however, semi-dilute solution behavior (*i.e.*, $\phi^* << \phi << 1$)[8] is more scientifically-interesting and relevant to application of these materials. Nanostructure scaling in semi-dilute solutions is more complicated because micelles impinge upon, and interact with, one another. As a result, copolymer concentration often impacts the dimensions of nanoscale features. This has been demonstrated via scattering experiments performed on semi-dilute diblock copolymer solutions[2,9,10] that quantify the ϕ dependence of r_A and of the center-to-center distance between micelles – d (= $2r_A + 2l_B$). Modification of dilute solution theory to consider higher concentrations[11] independently forecasts that r_A and l_B depend on ϕ. In general, experiments and theory agree that there is a slight, positive effect of ϕ on r_A whereas there is a

low to moderate, inverse effect of ϕ on d.[9–11] Semi-dilute solution theory further projects that scaling with N_A and N_B is still prevalent but unique from dilute solution behavior.[11]

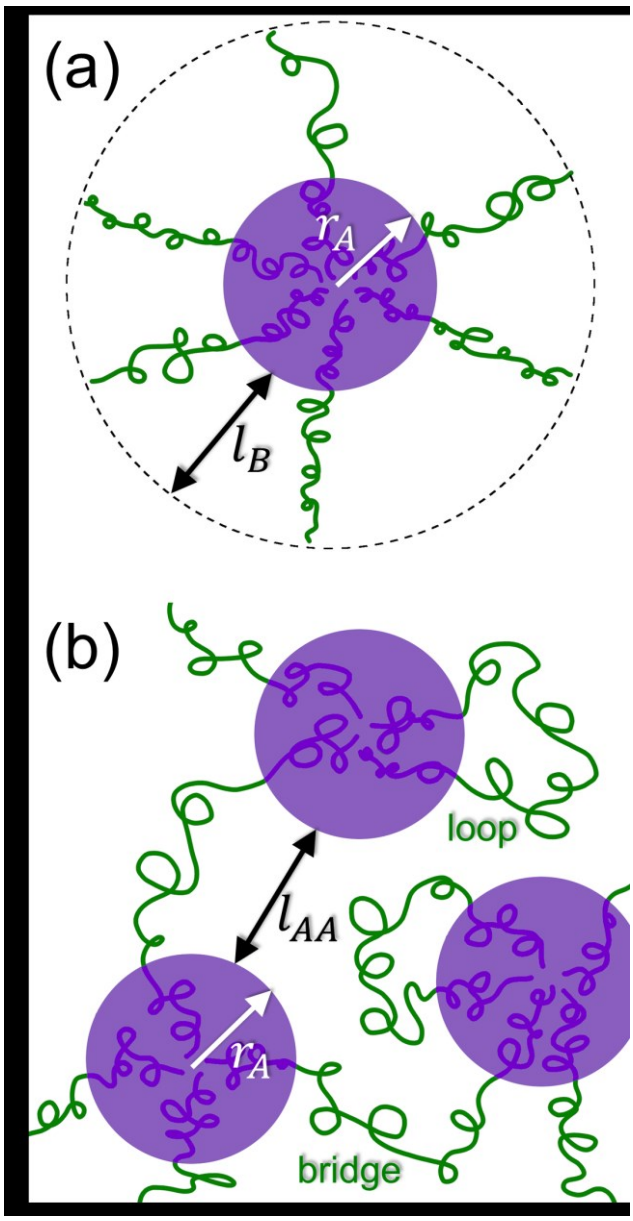

Figure 1. Schematic representation of a diblock copolymer micelle (a) and several triblock copolymer micelles in midblock selective solvent (b). Variables displayed in the figure include micelle core radius – r_A, micelle corona thickness – l_B, and intermicelle spacing – l_{AA}.

A logical progression from the study of diblock copolymer solution behavior discussed above is examination of symmetric ABA triblock copolymer solutions and gels. Solutions/gels of ABA triblock copolymers are similar in many ways to their diblock analogs. For example, ABA triblock copolymers dispersed in endblock-selective (A-selective) solvent exhibit micellar structure that is nearly indistinguishable from that of diblock copolymers (the sole exception being that both ends of the middle, B block are pinned to the core/corona interface).[12,13]

Micelles of ABA triblock copolymers at dilute concentration in midblock-selective (B-selective) solvent are also quite similar, but the coronal (B) blocks form loops (**Figure 1b**) with each end confined to the core/corona interface (often referred to as flower-like micelles).[14–16] The largest deviation of ABA triblock copolymer solution behavior occurs when present in midblock-selective solvent at concentrations in the semi-dilute regime. The adjacency of micelles enables midblocks to form bridges between neighboring micelles (**Figure 1b**), and the quantity of bridging midblocks increases with ϕ.[17–19] This molecular phenomenon leads to the formation of macroscopic gels even at modest concentrations ($\phi \sim 0.01$).[20–22] Limited experiments have shown that the scaling between d and ϕ in semi-dilute triblock copolymer gels is similar to semi-dilute diblock copolymer solutions.[23,24] However, scaling of nanostructural features in semi-dilute ABA triblock copolymer gels is mostly unexplored at this point both experimentally and theoretically. In particular, the effects of N_A, N_B, and ϕ on r_A and intermicelle spacing – l_{AA} – which is comparable to l_B, (**Figure 1b**) have not been determined. The objective of the current paper is to provide new experimental insight in this area.

2. Experimental Section

Materials: ABA triblock copolymer gels were prepared using aliphatic mineral oil (Sonneborn, Hyrobrite 200 PO) and one, or two, of several styrenic triblock copolymers (Kraton Corp. and Kuraray Co.). Molecular characteristics for each of the eight unique triblock copolymers used can be found in **Table 1**. Moving forward, the notation $S_xEB_yS_x$ and $S_xEP_yS_x$ is used to denote each copolymer where S represents a polystyrene block, EB represents a poly(ethylene-co-butylene) block, EP represents a poly(ethylene-co-propylene) block, and each subscript indicates the degree of polymerization for the corresponding block. Data used to calculate copolymer block degrees of polymerization are displayed in Table S1. Triblock copolymer gels were prepared by dissolving appropriate amounts of aliphatic mineral oil (MO) and desired triblock copolymer(s) in toluene (BDH, ≥99.5%) at a total concentration (*i.e.*, MO + copolymer) of 5 wt%. Fully dissolved solutions were then rotary evaporated to remove toluene and isolate the gel. Resultant gel was annealed in a vacuum oven at 140 °C and 0.95 atm vacuum for 18-24 hours and subsequently melt-pressed at 110-170 °C and minimal applied pressure to form uniform strips of *ca.* 1.6 mm thickness.

Table 1. Copolymer endblock (N_A) and midblock (N_B) degree of polymerization values for triblock copolymers used in the current study.

polymer	N_A	N_B
$S_{100}EB_{1560}S_{100}$	100 ± 3	1560 ± 53
$S_{161}EP_{2961}S_{161}$	161 ± 6	2961 ± 106
$S_{210}EB_{3177}S_{210}$	210 ± 11	3177 ± 159
$S_{218}EP_{5468}S_{218}$	218 ± 3	5468 ± 84
$S_{240}EP_{6710}S_{240}$	240 ± 10	6710 ± 282
$S_{348}EB_{4607}S_{348}$	348 ± 12	4607 ± 159
$S_{353}EP_{4944}S_{353}$	353 ± 4	4944 ± 58
$S_{588}EP_{9109}S_{588}$	588 ± 25	9109 ± 389

Small Angle X-ray Scattering: Small angle x-ray scattering (SAXS) measurements were conducted on beam line 12-ID-B at the Advanced Photon Source (APS) within Argonne National Laboratory. Experiments used 13.3 keV x-ray radiation (λ = 0.93 Å), a sample-to-detector distance of 2.01 m, and an exposure time of 1.0 s. Scattered x-rays were collected using a Pilatus 2M detector, and all measurements were performed at ambient temperature and pressure. Raw 2D data were converted into 1D profiles via azimuthal integration where the scattering vector magnitude, q, is related to the radiation wavelength and scattering half-angle, θ, by $q = 4\pi\sin(\theta)/\lambda$. One-dimensional scattering profiles were fit using SasView.[25]

Data Fitting: Select structural parameter sets were fit with a power law containing two independent variables (*i.e.*, $z = Ax^m y^n$ where A, m, and n are fitting constants) by pseudo-linearizing the equation ($\log(z) = \log(A) + m\log(x) + n\log(y)$) and subsequently fitting using MATLAB (Trust-Region-Reflective Algorithm). Remaining structural parameter sets were fit using a linearized, single-independent power law expression (*i.e.*, $\log(y) = \log(A) + m\log(x)$) and linear regression analysis.

3. Results and Discussion

3.1. SAXS Data & Modeling

In order to assess nanoscale structure, we collected and modeled small angle x-ray scattering (SAXS) data for each semi-dilute block copolymer gel considered. All of the raw 2D scattering patterns reflect isotropic behavior and thus we solely consider 1D data, which were acquired by azimuthal integration, as a sufficient descriptor of structure in these systems (**Figure 2a**). The

somewhat ambiguous 1D scattering data must be fit with a physically appropriate model in order to extract real-space structural information. We are confident that our gel formulations each exhibit spherical micelles surrounded by a midblock/solvent continuous phase based upon system parameter values (namely, $f_A\phi_{ABA} \leq 0.11$).[2,26] Spherical micelles are incorporated into the present scattering model using the spherical form factor, $P(q)$, expression

$$P(q) = \left(3\left(\frac{4}{3}\pi r_A^3\right)\frac{\sin(qr_A) - qr_A\cos(qr_A)}{(qr_A)^3}\right)^2 \quad (1)$$

where r_A is the micelle core radius. We anticipate that there is some distribution of micelle size present in gels and use a Schulz distribution, which contains an average r_A and its polydispersity $\equiv PD$, to expand upon Equation 1.[25] In the remainder of this paper, all values reported are the average r_A. (*PD* values were held constant within a gel series comprised of the same copolymer and ranged overall from 0.09 to 0.12.)

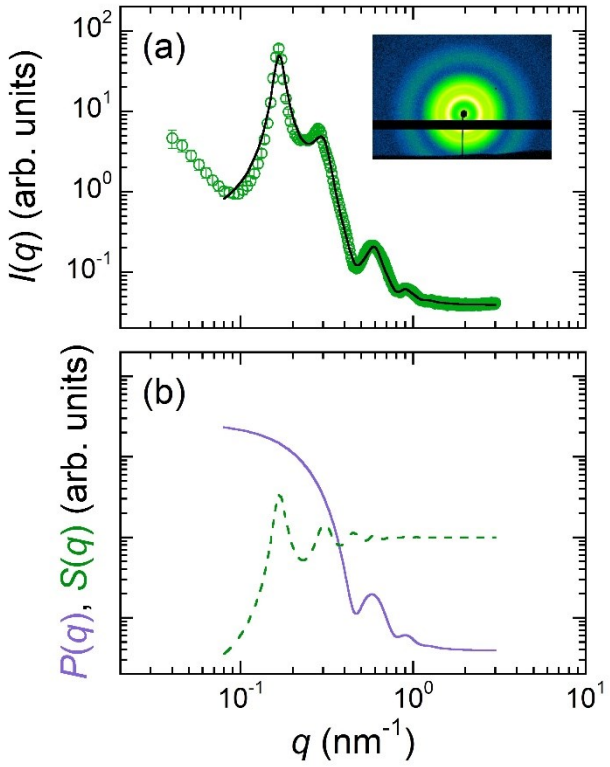

Figure 2. In (a), an example of a 2D SAXS pattern for a semi-dilute block copolymer gel (inset), the corresponding 1D SAXS profile (data points), and the modified hard sphere model fit (solid line). In (b), the form factor – $P(q)$ – (solid line) and structure factor – $S(q)$ – (dashed line) contributions of the modified hard sphere model. This particular fit reflects r_A = 9.6 nm, l_{AA} = 22.8 nm, and ϕ_A = 0.049.

The moderate concentration of block copolymer, and hence compactness of the nanoscale structure, results in interdomain scattering interference that is dependent on the spacing between the spherical micelles. This is incorporated into the present scattering model using a hard sphere structure factor, $S(q)$, of the form

$$S(q) = 1 + 4\pi\left(\frac{\phi_{hs}}{4\pi r_{hs}^3/3}\right)\int_0^\infty (g(r)-1)\left(\frac{\sin(qr)}{qr}\right)r^2 dr \quad (2)$$

where r_{hs} is the hard sphere radius (*i.e.*, half of the center-to-center distance between spherical domains), ϕ_{hs} is the volume fraction of these hard spheres, and $g(r)$ is their radial distribution function, which is further expressed as

$$g(r) = \exp(-U(r)/k_B T) \quad (3)$$

and the interaction potential, $U(r)$, is

$$U(r) = \begin{cases} \infty & r < 2r_{hs} \\ 0 & r \geq 2r_{hs} \end{cases} \quad (4)$$

The intermicelle spacing, l_{AA}, can be derived from the $S(q)$ and $P(q)$ pieces of the model via $2r_{hs} - 2r_A$ as can the volume fraction of A-block micelles, ϕ_A (= $\phi_{hs}(r_A/r_{hs})^3$). Finally, the overall expression for scattering intensity, $I(q)$, is expressed by combining Equations 1 and 2 and accounting for incoherent background scattering, *bkg*, using

$$I(q) = \beta P(q) S(q) + bkg \quad (5)$$

where β is a weighting factor that depends on electron density contrast between the micelles and the continuous phase, as well as, the number density of micelles.[27] We refer to Equation 5 with inputs from Equations 1 and 2 as the modified hard sphere model.

It is clear from comparing the fitted modified hard sphere model with experimental scattering data (**Figure 2a** and Figures S1 and S2) that Equation 5 is an appropriate choice for the current systems. It is also reassuring, in terms of confidence in fitting parameters, that the form factor and structure factor contributions each have a meaningful influence on the overall model (**Figure 2b**). Beyond these corroborations, we quantitatively validated the use of this model by comparing the experimentally-determined ϕ_A, which is now referred to as $\phi_{A,SAXS}$, with that anticipated based upon copolymer and formulation parameters, $\phi_{A,form}$ (= $\phi_{ABA} f_A \rho_{ABA}/\rho_A$). We find excellent agreement between $\phi_{A,SAXS}$ and $\phi_{A,form}$ for all gels analyzed (Figures S3 and S4).

3.2. Nanostructure Scaling Analysis

The r_A and l_{AA} values extracted from SAXS analysis for the variety of formulated gels span a relatively wide range (**Figure 3a** and **Figure 3b**). It is also apparent that each geometric parameter is dependent on both concentration and copolymer identity. In the former case, increasing copolymer concentration leads to increased micelle size and decreased intermicelle spacing regardless of the copolymer used in gel formulation. Concerning copolymer identity, general trends are not as straightforward because the copolymer block lengths are not varied independently of one another. It is, however, possible to see that the largest copolymer ($S_{588}EP_{9109}S_{588}$) exhibits the largest micelles and intermicelle spacings across all concentrations and that the smallest copolymer ($S_{100}EB_{1560}S_{100}$) exhibits the smallest micelles and intermicelle spacings.

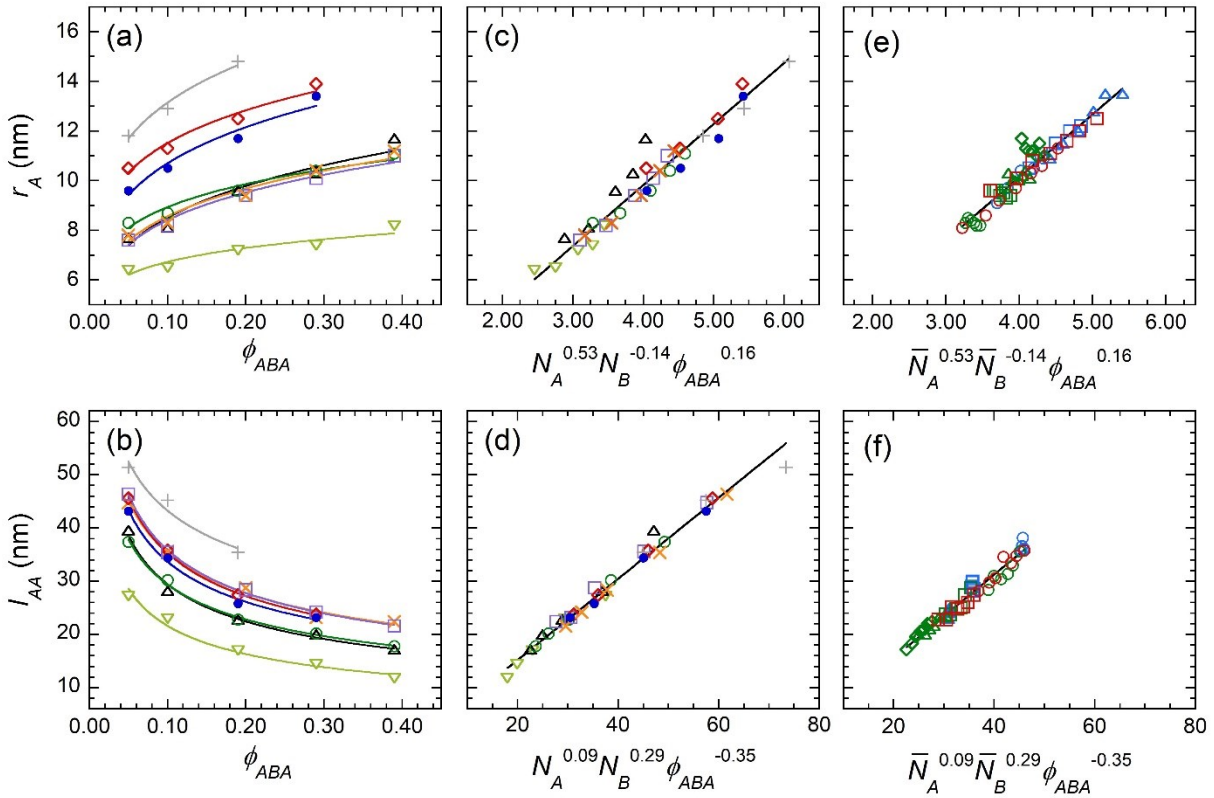

Figure 3. Spherical domain radius, r_A, as a function of copolymer concentration (a) and rescaled variables (c) for gels containing a single triblock copolymer and for systems containing two triblock copolymers as a function of rescaled variables (e). Additionally, intermicelle spacing, l_{AA}, as a function of copolymer concentration (b) and rescaled variables (d) for gels containing a single triblock copolymer and for systems containing two triblock copolymers as a function of rescaled variables (f). In (a)-(d), $S_{100}EB_{1560}S_{100}$: light green ▽, $S_{161}EP_{2961}S_{161}$: black △, $S_{210}EB_{3177}S_{210}$: green ○, $S_{218}EP_{5468}S_{218}$: purple □, $S_{240}EP_{6710}S_{240}$: orange x, $S_{348}EB_{4607}S_{348}$: blue ●, $S_{353}EP_{4944}S_{353}$: red ◇, $S_{588}EP_{9109}S_{588}$: gray +. In (e) and (f), $S_{218}EP_{5468}S_{218}$ and $S_{353}EP_{4944}S_{353}$:

blue, $S_{353}EP_{4944}S_{353}$ and $S_{161}EP_{2961}S_{161}$: red, $S_{218}EP_{5468}S_{218}$ and $S_{161}EP_{2961}S_{161}$: green; ϕ_{ABA} = 0.10: ○, ϕ_{ABA} = 0.19: □, ϕ_{ABA} = 0.29: △, ϕ_{ABA} = 0.39: ◇. In (a) and (b), solid lines are power law fits to each copolymer series. In (c)-(f), solid lines are linear fits with a *y*-intercept of zero.

In order to evaluate whether nanostructural scaling relationships in formulated gels can be universally described, we assume that the effects of ϕ_{ABA}, N_A, and N_B are non-interacting. This enables data to be considered one or two parameters at a time. First, we assess the scaling between each structural parameter and copolymer concentration. Sets of r_A and l_{AA} data for gels with fixed copolymer identity were fitted to a power law (**Figure 3a** and **Figure 3b**) and the fitted exponent and corresponding standard deviation were recorded (Table S2). Analysis of these results indicates that there is not a significant difference in scaling exponents for either structural feature (r_A: p = 0.264, l_{AA}: p = 0.352, ANOVA) and that the overall scaling relationships are $r_A \sim \phi_{ABA}^{0.16\pm0.04}$ and $l_{AA} \sim \phi_{ABA}^{-0.35\pm0.03}$. Next, we consider the scaling between each structural parameter and copolymer block lengths – N_A and N_B – at fixed concentration. The copolymers employed do not allow complete separation of these two parameters and so the fitted exponents are determined simultaneously using $r_A \sim N_A^w N_B^x$ and $l_{AA} \sim N_A^y N_B^z$. Once again, fitted exponents and corresponding standard deviation for each fixed copolymer concentration set were recorded (Table S3). No significant difference between sets was detected (w: p = 0.558, x: p = 0.473, y: p = 0.053, z: p = 0.055, ANOVA), and the yielded scaling relationships are $r_A \sim N_A^{0.53\pm0.07} N_B^{-0.14\pm0.07}$ and $l_{AA} \sim N_A^{0.09\pm0.08} N_B^{0.29\pm0.07}$. Altogether, the scaling of nanoscale structural parameters assuming non-interacting factors are given by

$$r_A \sim N_A^{(0.53\pm0.07)} N_B^{(-0.14\pm0.07)} \phi_{ABA}^{(0.16\pm0.04)} \quad (6)$$

$$l_{AA} \sim N_A^{(0.09\pm0.08)} N_B^{(0.29\pm0.07)} \phi_{ABA}^{(-0.35\pm0.03)} \quad (7)$$

Further endorsement of Equations 6 and 7 is provided by replotting each structural parameter against the appropriately scaled and combined dependencies (**Figure 3c** and **Figure 3d**). There is outstanding agreement between the determined scaling behavior and experimental data as reflected by visual inspection and quality of fits (r_A: R^2 = 0.970, l_{AA}: R^2 = 0.992). We therefore conclude that the assumption of non-interacting parameters is valid and that Equations 6 and 7 reflect the scaling behavior for all gel systems considered.

In an attempt to further investigate the generality of Equations 6 and 7, we formulated several gels containing two of the copolymers listed in **Table 1** – namely, $S_{218}EP_{5468}S_{218}$/$S_{353}EP_{4944}S_{353}$, $S_{353}EP_{4944}S_{353}$/$S_{161}EP_{2961}S_{161}$, and $S_{218}EP_{5468}S_{218}$/ $S_{161}EP_{2961}S_{161}$ – in varying ratios (ϕ_1/ϕ_2 = 1/1, 2/1, 1/2, 4/1, and 1/4) and total copolymer concentrations ($\phi_{ABA} = \phi_1 + \phi_2$ = 0.10, 0.19, 0.29, and

0.39). Depending on the specific pairing, r_A and/or l_{AA} varies with the ratio ϕ_1/ϕ_2 at a fixed total copolymer concentration (Figure S5). This variation most likely arises from the evolution in the average block lengths – $\overline{N}_A$ and $\overline{N}_B$ – over the range of ϕ_1/ϕ_2 where $\overline{N}_i = (N_{i,1}\phi_1 + N_{i,2}\phi_2)/(\phi_1 + \phi_2)$ and $N_{i,1}$ and $N_{i,2}$ are the i block lengths for copolymer 1 and 2, respectively. The structural parameters determined for gels containing two triblock copolymers are plotted against the scaling presented in Equations 6 and 7 with N_A and N_B being replaced by $\overline{N}_A$ and $\overline{N}_B$ (**Figure 3e** and **Figure 3f**). Clearly, the previous scaling results hold for these gels as supported visually and by quality of fits (r_A: $R^2 = 0.966$, l_{AA}: $R^2 = 0.985$).

3.3. Discussion of Scaling Results

There are no published scaling theories for semi-dilute ABA triblock copolymer gels at the current point in time. Therefore, we compare our observations with theory for semi-dilute diblock copolymer solutions. The model of Birshtein and Zhulina[11] frames geometric parameter scaling using several concentration regimes. The lowest concentration regime is that for dilute diblock copolymer solutions, and is irrelevant here. The second regime consists of diblock copolymers at moderate concentration (*ca.* $0.01 \leq \phi_{ABA} \leq 0.30$) and is defined by copolymer concentrations which yield micelles that interact at the periphery of their coronas but do not have overlapping (*i.e.*, interpenetrating) coronal chains. In this regime, the size of the micelle cores is independent of concentration (*i.e.*, $r_A \sim N_A^{3/5}$) and the corona layer thickness follows concentration scaling based upon geometric considerations (*i.e.*, $l_B \sim N_A^{1/3}N_B^{4/15}\phi_{ABA}^{-1/3}$). The highest concentration regime ($\phi_{ABA} > 0.30$) consists of micelles with interpenetrating coronal chains, which causes considerable restructuring of the corona layer and, as a result, micelle core size depends on concentration (*i.e.*, $r_A \sim N_A^{2/3}\phi_{ABA}^{0.26}$). There is also a dampened effect of concentration on corona thickness (*i.e.*, $l_B \sim N_A^{1/3}N_B^{1/3}\phi_{ABA}^{-0.08}$) in the high concentration regime due to increased crowding of micelles.

While almost all of the considered ABA triblock copolymer gels exist in the moderate concentration regime as it is defined by Reference 11, the difference in molecular structure between triblock and diblock copolymers complicates the distinction between the previously defined moderate and high concentration regimes. Specifically, triblock copolymers naturally have interpenetrating coronas even at moderate concentrations due to bridging midblocks. We hypothesize that this difference manifests itself through a balance of the moderate and high concentration regime geometric scaling relationships discussed in the previous paragraph. First, the presence of bridging causes restructuring of the corona layer (compared to diblock copolymer micelles at moderate concentration) and so we anticipate that r_A would scale in a

similar fashion to the high diblock concentration regime. Our hypothesis is supported through the modest agreement between our results and those from theory for high diblock copolymer concentration ($\sim N_A^{0.53} N_B^{-0.14} \phi_{ABA}^{0.16}$ vs. $\sim N_A^{2/3} \phi_{ABA}^{0.26}$). Second, we postulate that the actual concentration of copolymer molecules, and consequently of A-rich micelles, is the dominant factor affecting l_{AA} since micelle crowding is the cited explanation for the dampened impact of ϕ on corona thickness. This leads to the anticipation that l_{AA} scales similarly to l_B in the moderate diblock concentration regime, which is also supported by modest agreement between our results and theory ($l_{AA} \sim N_A^{0.09} N_B^{0.29} \phi_{ABA}^{-0.35}$ vs. $l_B \sim N_A^{1/3} N_B^{4/15} \phi_{ABA}^{-1/3}$). Although the majority of scaling relationships seem to be captured using diblock copolymer scaling theory, we note that r_A is more dependent on N_B and l_{AA} is less dependent on N_A than semi-dilute diblock theory suggests. This likely reflects a need to consider additional contributions from the triblock copolymer free energy landscape such as the energetics of looping and bridging midblocks and the fraction of chains that form bridges versus loops.

4. Conclusion

Analysis of scattering data indicates that the nanostructure of ABA triblock copolymer gels can be universally described through appropriate scaling of copolymer block lengths and concentration (Equations 6 and 7). Furthermore, the determined scaling dependencies are somewhat in line with predictions from semi-dilute diblock copolymer solution theory. Though these correlations are promising, we expect that scaling theory specifically developed for semi-dilute triblock copolymer solutions (in B-selective solvent) would better capture the full scaling behavior observed. More specifically, the conformational free energy of triblock copolymer midblock bridges and loops must be considered along with the population of each. In the future, we hope that the development of such theory will enable us to better understand the present scaling behavior.

Supporting Information

Supporting Information is available from the Wiley Online Library.

Acknowledgements

This work was supported by the National Science Foundation under Grant No. 1904047. We would like to thank Kraton, Kuraray, and Sonneborn for providing the copolymers and aliphatic oil used in this study, as well as, Byeongdu Lee and Ivan Kuzmenko for SAXS experimental

support. This research used resources of the Advanced Photon Source, a U.S. Department of Energy (DOE) Office of Science user facility, operated for the DOE Office of Science by Argonne National Laboratory under Contract No. DE-AC02-06CH11357. Extraordinary facility operations were supported in part by the DOE Office of Science through the National Virtual Biotechnology Laboratory, a consortium of DOE national laboratories focused on the response to COVID-19, with funding provided by the Coronavirus CARES Act.

Received: ((will be filled in by the editorial staff))
Revised: ((will be filled in by the editorial staff))
Published online: ((will be filled in by the editorial staff))

References

(1) Hamley, I. W. *Block Copolymers in Solution: Fundamentals and Applications*; John Wiley & Sons, 2005.

(2) Hanley, K. J.; Lodge, T. P.; Huang, C.-I. Phase Behavior of a Block Copolymer in Solvents of Varying Selectivity. *Macromolecules* **2000**, *33* (16), 5918–5931. https://doi.org/10.1021/ma000318b.

(3) Lodge, T. P.; Pudil, B.; Hanley, K. J. The Full Phase Behavior for Block Copolymers in Solvents of Varying Selectivity. *Macromolecules* **2002**, *35* (12), 4707–4717. https://doi.org/10.1021/ma0200975.

(4) de Gennes, P. G. Macromolecules and Liquid Crystals: Reflections on Certain Lines of Research. In *Liquid Crystals (Solid State Physics Supplements 14)*; Academic Press: New York, 1978.

(5) Zhulina, Ye. B.; Birshtein, T. M. Conformations of Block-Copolymer Molecules in Selective Solvents (Micellar Structures. *Polymer Science U.S.S.R.* **1985**, *27* (3), 570–578. https://doi.org/10.1016/0032-3950(85)90238-2.

(6) Whitmore, M. D.; Noolandi, J. Theory of Micelle Formation in Block Copolymer-Homopolymer Blends. *Macromolecules* **1985**, *18* (4), 657–665. https://doi.org/10.1021/ma00146a014.

(7) Nagarajan, R.; Ganesh, K. Block Copolymer Self-assembly in Selective Solvents: Spherical Micelles with Segregated Cores. *J. Chem. Phys.* **1989**, *90* (10), 5843–5856. https://doi.org/10.1063/1.456390.

(8) Gennes, P.-G. de. *Scaling Concepts in Polymer Physics*; Cornell University Press, 1979.

(9) Shibayama, M.; Hashimoto, T.; Kawai, H. Ordered Structure in Block Polymer Solutions. 1. Selective Solvents. *Macromolecules* **1983**, *16* (1), 16–28. https://doi.org/10.1021/ma00235a005.

(10) Lai, C.; Russel, W. B.; Register, R. A. Scaling of Domain Spacing in Concentrated Solutions of Block Copolymers in Selective Solvents. *Macromolecules* **2002**, *35* (10), 4044–4049. https://doi.org/10.1021/ma0122223.

(11) Birshtein, T. M.; Zhulina, E. B. Scaling Theory of Supermolecular Structures in Block Copolymer-Solvent Systems: 1. Model of Micellar Structures. *Polymer* **1989**, *30* (1), 170–177. https://doi.org/10.1016/0032-3861(89)90399-6.

(12) Birshtein, T. M.; Zhulina, E. B. Scaling Theory of Supermolecular Structures in Block Copolymer-Solvent Systems: 2. Supercrystalline Structures. *Polymer* **1990**, *31* (7), 1312–1320. https://doi.org/10.1016/0032-3861(90)90223-L.

(13) Zhulina, E. B.; Borisov, O. V. Theory of Block Polymer Micelles: Recent Advances and Current Challenges. *Macromolecules* **2012**, *45* (11), 4429–4440. https://doi.org/10.1021/ma300195n.

(14) Ten Brinke, G.; Hadziioannou, G. Topological Constraints and Their Influence on the Properties of Synthetic Macromolecular Systems. 2. Micelle Formation of Triblock Copolymers. *Macromolecules* **1987**, *20* (3), 486–489. https://doi.org/10.1021/ma00169a004.

(15) Balsara, N. P.; Tirrell, M.; Lodge, T. P. Micelle Formation of BAB Triblock Copolymers in Solvents That Preferentially Dissolve the A Block. *Macromolecules* **1991**, *24* (8), 1975–1986. https://doi.org/10.1021/ma00008a040.

(16) de Graaf, A. J.; Boere, K. W. M.; Kemmink, J.; Fokkink, R. G.; van Nostrum, C. F.; Rijkers, D. T. S.; van der Gucht, J.; Wienk, H.; Baldus, M.; Mastrobattista, E.; Vermonden, T.; Hennink, W. E. Looped Structure of Flowerlike Micelles Revealed by 1H NMR Relaxometry and Light Scattering. *Langmuir* **2011**, *27* (16), 9843–9848. https://doi.org/10.1021/la2019605.

(17) Watanabe, H.; Sato, T.; Osaki, K. Concentration Dependence of Loop Fraction in Styrene−Isoprene−Styrene Triblock Copolymer Solutions and Corresponding Changes in Equilibrium Elasticity. *Macromolecules* **2000**, *33* (7), 2545–2550. https://doi.org/10.1021/ma991979f.

(18) Sliozberg, Y. R.; Andzelm, J. W.; Brennan, J. K.; Vanlandingham, M. R.; Pryamitsyn, V.; Ganesan, V. Modeling Viscoelastic Properties of Triblock Copolymers: A DPD Simulation Study. *Journal of Polymer Science Part B: Polymer Physics* **2010**, *48* (1), 15–25. https://doi.org/10.1002/polb.21839.

(19) Mineart, K. P.; Vallely, M. J.; Rankin, L. A.; Hill, D. M.; Lee, B. Implications of Styrenic Triblock Copolymer Gel Mechanics on Midblock Bridging Fraction. *Polymer* **2022**, *260*, 125394. https://doi.org/10.1016/j.polymer.2022.125394.

(20) Laurer, J. H.; Mulling, J. F.; Khan, S. A.; Spontak, R. J.; Bukovnik, R. Thermoplastic Elastomer Gels. I. Effects of Composition and Processing on Morphology and Gel Behavior. *J. Polym. Sci. B Polym. Phys.* **1998**, *36* (13), 2379–2391. https://doi.org/10.1002/(SICI)1099-0488(19980930)36:13<2379::AID-POLB13>3.0.CO;2-0.

(21) Laurer, J. H.; Mulling, J. F.; Khan, S. A.; Spontak, R. J.; Lin, J. S.; Bukovnik, R. Thermoplastic Elastomer Gels. II. Effects of Composition and Temperature on Morphology and Gel Rheology. *J. Polym. Sci. Pt. B-Polym. Phys.* **1998**, *36* (14), 2513–2523.

(22) Vega, D. A.; Sebastian, J. M.; Loo, Y.-L.; Register, R. A. Phase Behavior and Viscoelastic Properties of Entangled Block Copolymer Gels. *Journal of Polymer Science Part B: Polymer Physics* **2001**, *39* (18), 2183–2197. https://doi.org/10.1002/polb.1192.

(23) Lairez, D.; Adam, M.; Raspaud, E.; Carton, J.-P.; Bouchaud, J.-P. Triblock Copolymers in a Selective Solvent: Dilute and Semi-Dilute Solutions. *Macromolecular Symposia* **1995**, *90* (1), 203–229. https://doi.org/10.1002/masy.19950900117.

(24) Raspaud, E.; Lairez, D.; Adam, M.; Carton, J.-P. Triblock Copolymers in a Selective Solvent. 2. Semidilute Solutions. *Macromolecules* **1996**, *29* (4), 1269–1277. https://doi.org/10.1021/ma951172x.

(25) Doucet, M.; Cho, J. H.; Alina, G.; Attala, Z.; Bakker, J.; Bouwman, W.; Butler, P.; Campbell, K.; Cooper-Benun, T.; Durniak, C.; Forster, L.; Gonzales, M.; Heenan, R.; Jackson, A.; King, S.; Kienzle, P.; Krzywon, J.; Nielsen, T.; O'Driscoll, L.; Potrzebowski, W.; Prescott, S.; Ferraz Leal, R.; Rozycko, P.; Snow, T.; Washington, A. SasView Version 5.0.3, 2020. https://doi.org/10.5281/zenodo.3930098.

(26) Woloszczuk, S.; Tuhin, M. O.; Gade, S. R.; Pasquinelli, M. A.; Banaszak, M.; Spontak, R. J. Complex Phase Behavior and Network Characteristics of Midblock-Solvated Triblock Copolymers as Physically Cross-Linked Soft Materials. *ACS Appl. Mater. Interfaces* **2017**, *9* (46), 39940–39944. https://doi.org/10.1021/acsami.7b14298.

(27) Kinning, D. J.; Thomas, E. L. Hard-Sphere Interactions between Spherical Domains in Diblock Copolymers. *Macromolecules* **1984**, *17* (9), 1712–1718. https://doi.org/10.1021/ma00139a013.

Nanostructure Scaling in Semi-Dilute Block Copolymer Gels

Kenneth P. Mineart,* Matthew J. Vallely, Emma K. O'Shea

Table of Contents Entry

Small angle x-ray scattering enables the measurement of ABA triblock copolymer gel nanostructure dimensions, specifically the radius of spherical domains and the spacing between them. Subsequent analysis of these dimensions yields a universal scaling expression for sphere radius and for intermicelle spacing based upon triblock copolymer block lengths and concentration within the gel.

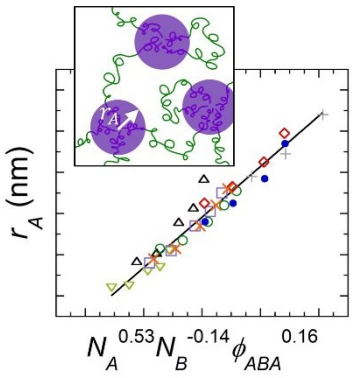

Supporting Information

Nanostructure Scaling in Semi-Dilute Block Copolymer Gels

Kenneth P. Mineart,* Matthew J. Vallely, Emma K. O'Shea

Table S1. Copolymer parameters used in determining block degree of polymerization values.

polymer	M_w[a] **[kg/mol]**	f_S[b] **[g S/g]**	f_E[b] **[g E/g]**	f_P[b] **[g P/g]**	f_B[b] **[g B/g]**
$S_{100}EB_{1560}S_{100}$	75.9 ± 2.6	0.275	0.428	-	0.297
$S_{161}EP_{2961}S_{161}$	129.0 ± 4.6	0.260	0.452	0.288	-
$S_{210}EB_{3177}S_{210}$	157.5 ± 7.9	0.278	0.410	-	0.312
$S_{218}EP_{5468}S_{218}$	241.1 ± 3.7	0.188	0.285	0.527	-
$S_{240}EP_{6710}S_{240}$	286.0 ± 12.0	0.175	0.325	0.500	-
$S_{348}EB_{4607}S_{348}$	234.9 ± 8.1	0.309	0.410	-	0.281
$S_{353}EP_{4944}S_{353}$	247.8 ± 2.9	0.297	0.274	0.429	-
$S_{588}EP_{9109}S_{588}$	421.0 ± 18.0	0.291	0.403	0.306	-

[a] M_w values were determined via static light scattering measurements; [b] f_S (styrene), f_E (ethylene), f_P (propylene), or f_B (butylene) values were determined via H^1-NMR.

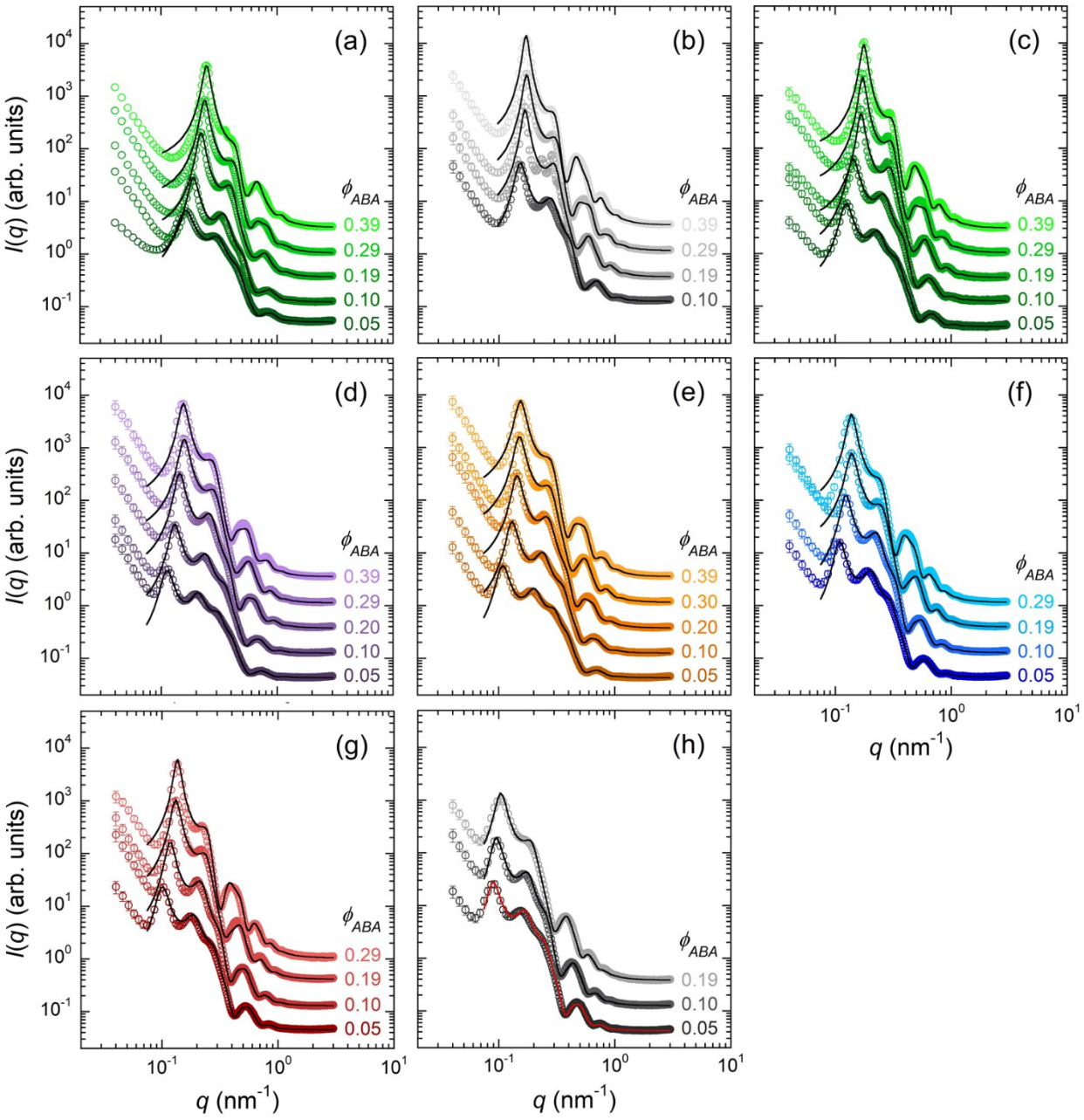

Figure S1. Representative 1D SAXS data from gels composed of various ABA triblock copolymers at different concentrations (values indicated on each plot): (a) $S_{100}EB_{1560}S_{100}$, (b) $S_{161}EP_{2961}S_{161}$, (c) $S_{210}EB_{3177}S_{210}$, (d) $S_{218}EP_{5468}S_{218}$, (e) $S_{240}EP_{6710}S_{240}$, (f) $S_{348}EB_{4607}S_{348}$, (g) $S_{353}EP_{4944}S_{353}$ and (h) $S_{588}EP_{9109}S_{588}$. Data are vertically-shifted by a factor of 3^n for clarity and solid lines are fits using the modified hard sphere model.

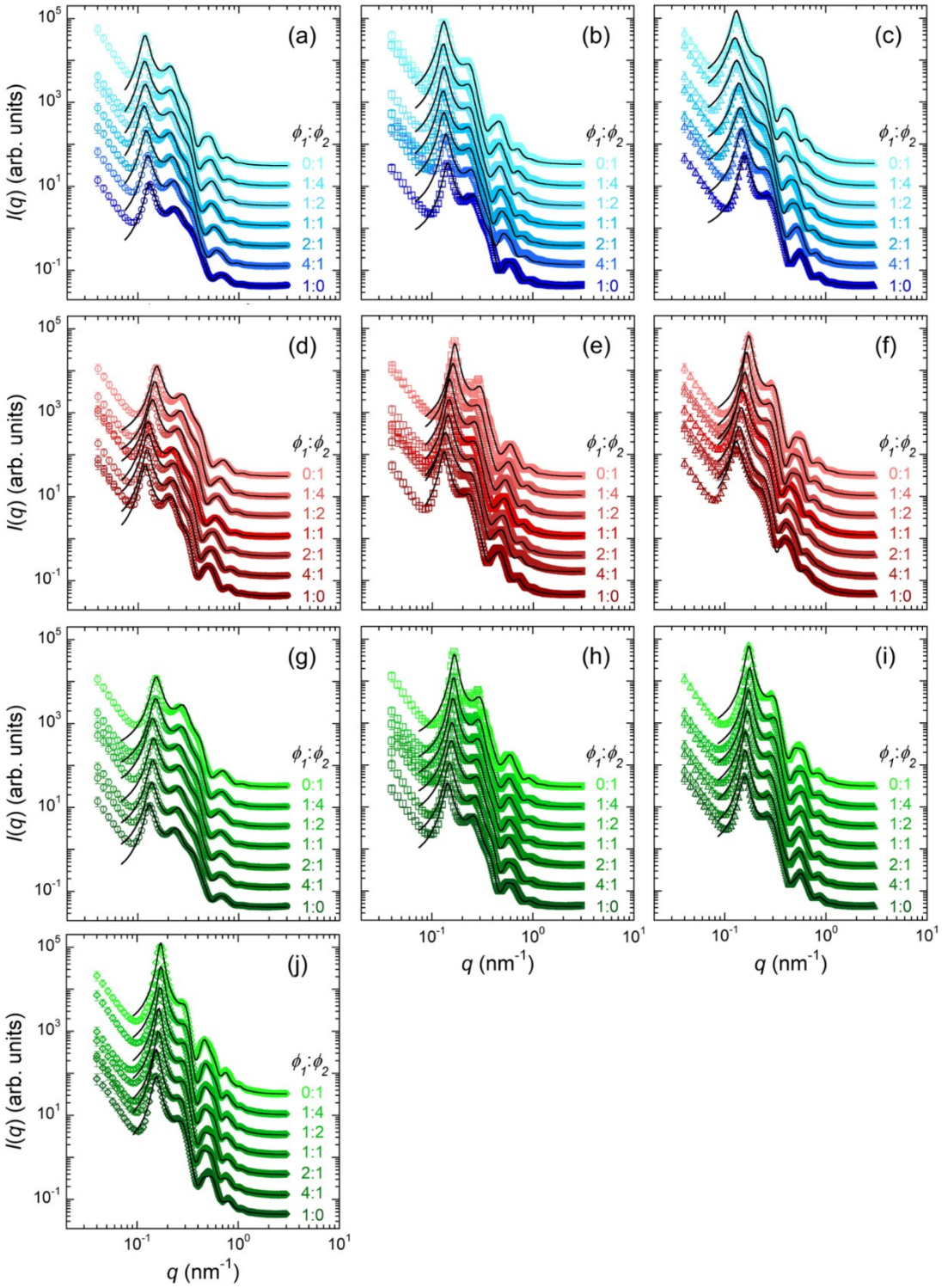

Figure S2. Representative 1D SAXS data from gels composed of pairs of ABA triblock copolymers at different ratios (ϕ_1:ϕ_2 indicated on each plot) and different total copolymer concentrations ($\phi_{ABA} = \phi_1 + \phi_2$): $S_{218}EP_{5468}S_{218}$ and $S_{353}EP_{4944}S_{353}$ at $\phi_{ABA} = 0.10$ (a), $\phi_{ABA} = 0.19$ (b), and $\phi_{ABA} = 0.29$ (c); $S_{353}EP_{4944}S_{353}$ and $S_{161}EP_{2961}S_{161}$ at $\phi_{ABA} = 0.10$ (d), $\phi_{ABA} = 0.19$ (e), and $\phi_{ABA} = 0.29$ (f); and $S_{218}EP_{5468}S_{218}$ and $S_{161}EP_{2961}S_{161}$ at $\phi_{ABA} = 0.10$ (g), $\phi_{ABA} = 0.19$ (h), $\phi_{ABA} = 0.29$ (i), and $\phi_{ABA} = 0.39$ (j). Data are vertically-shifted by a factor of 3^n for clarity and solid lines are fits using the modified hard sphere model.

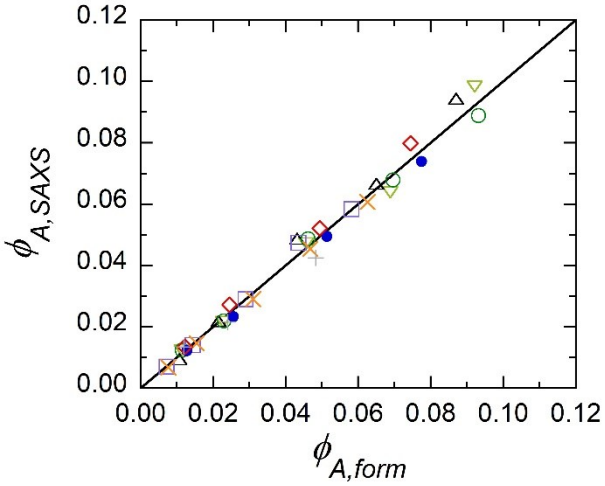

Figure S3. Comparison between the endblock volume fraction anticipated from formulation quantities, $\phi_{A,form}$, and that calculated from modified hard sphere fits of SAXS profiles, $\phi_{A,SAXS}$. Data are shown for all triblock copolymer gels analyzed and the solid line indicates quantitative agreement ($S_{100}EB_{1560}S_{100}$: light green ▽, $S_{161}EP_{2961}S_{161}$: black △, $S_{210}EB_{3177}S_{210}$: green ○, $S_{218}EP_{5468}S_{218}$: purple □, $S_{240}EP_{6710}S_{240}$: orange x, $S_{348}EB_{4607}S_{348}$: blue ●, $S_{353}EP_{4944}S_{353}$: red ◇, $S_{588}EP_{9109}S_{588}$: gray +).

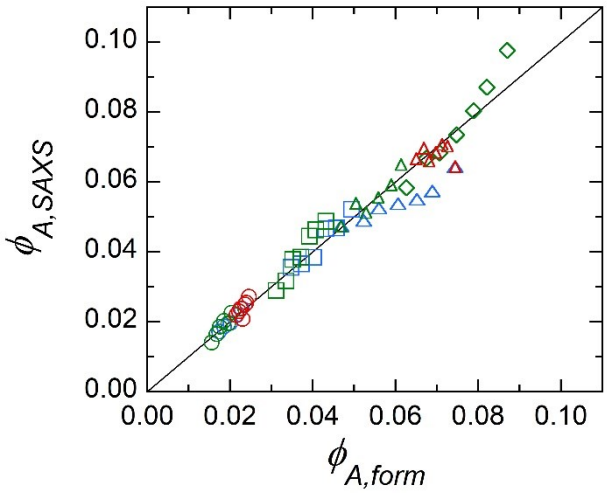

Figure S4. Comparison between the endblock volume fraction anticipated from formulation quantities, $\phi_{A,form}$, and that calculated from modified hard sphere fits of SAXS profiles, $\phi_{A,SAXS}$. Data are shown for all gels containing two triblock copolymers and the solid line indicates quantitative agreement ($S_{218}EP_{5468}S_{218}$ and $S_{353}EP_{4944}S_{353}$: blue, $S_{353}EP_{4944}S_{353}$ and $S_{161}EP_{2961}S_{161}$: red, $S_{218}EP_{5468}S_{218}$ and $S_{161}EP_{2961}S_{161}$: green; $\phi_{ABA} = 0.10$: ○, $\phi_{ABA} = 0.19$: □, $\phi_{ABA} = 0.29$: △, $\phi_{ABA} = 0.39$: ◇).

Table S2. Fitted scaling exponents – m and n (where $r_A \sim \phi_{ABA}^m$ and $l_{AA} \sim \phi_{ABA}^n$) – for individual copolymer series and corresponding standard deviation values.

polymer	***m***	***n***
$S_{100}EB_{1560}S_{100}$	0.11 ± 0.04	-0.40 ± 0.05
$S_{161}EP_{2961}S_{161}$	0.20 ± 0.05	-0.38 ± 0.04
$S_{210}EB_{3177}S_{210}$	0.14 ± 0.03	-0.36 ± 0.02
$S_{218}EP_{5468}S_{218}$	0.18 ± 0.05	-0.35 ± 0.04
$S_{240}EP_{6710}S_{240}$	0.18 ± 0.03	-0.34 ± 0.03
$S_{348}EB_{4607}S_{348}$	0.15 ± 0.05	-0.36 ± 0.01
$S_{353}EP_{4944}S_{353}$	0.17 ± 0.03	-0.36 ± 0.02
$S_{588}EP_{9109}S_{588}$	0.16 ± 0.13	-0.27 ± 0.04
overall	**0.16 ± 0.04**	**-0.35 ± 0.03**

Table S3. Fitted scaling exponents – w, x, y, and z (where $r_A \sim N_A^w N_B^x$ and $l_{AA} \sim N_A^y N_B^z$) – for individual concentration series and corresponding standard deviation values. Note, the exponents from ϕ_{ABA} = 0.39 were not used in overall analysis due to their considerable uncertainty.

ϕ_{ABA}	w	x	y	z
0.05	0.51 ± 0.07	-0.17 ± 0.07	0.04 ± 0.11	0.31 ± 0.10
0.10	0.54 ± 0.06	-0.16 ± 0.06	0.14 ± 0.06	0.24 ± 0.06
0.19	0.50 ± 0.10	-0.12 ± 0.09	0.05 ± 0.08	0.35 ± 0.07
0.29	0.56 ± 0.13	-0.12 ± 0.11	0.13 ± 0.09	0.27 ± 0.08
0.39	0.47 ± 0.88	-0.09 ± 0.54	0.29 ± 0.58	0.27 ± 0.35
overall	**0.53 ± 0.07**	**-0.14 ± 0.07**	**0.09 ± 0.08**	**0.29 ± 0.07**

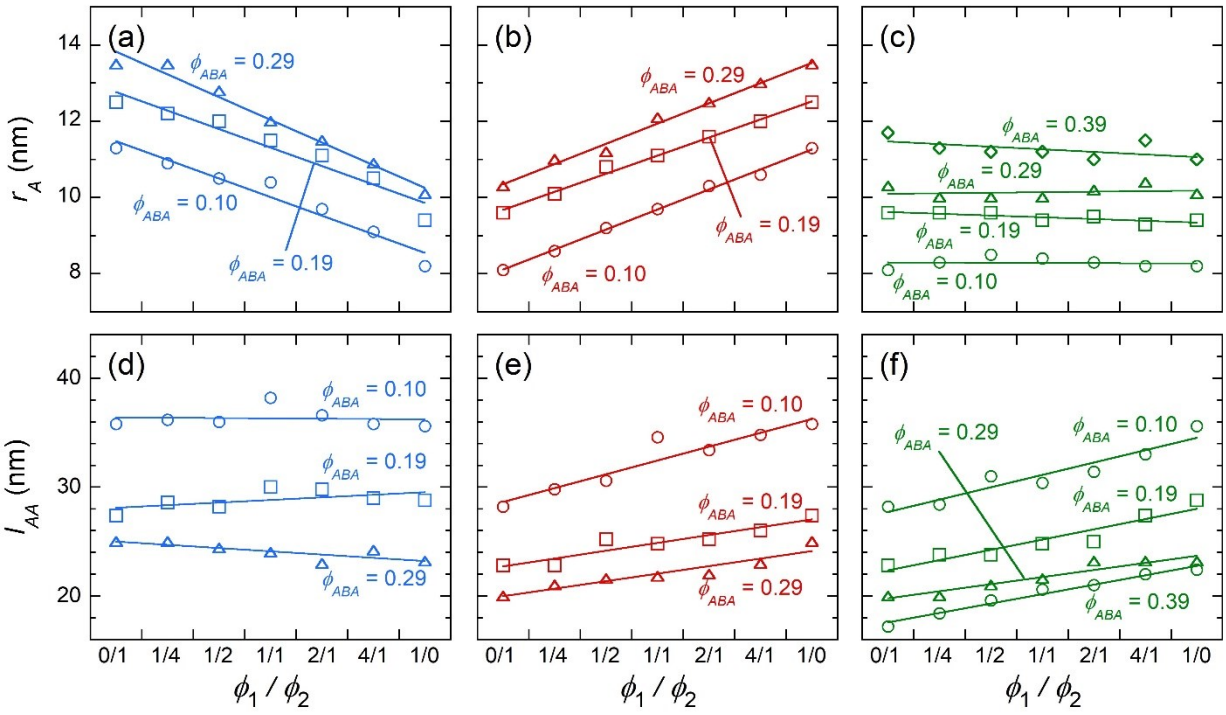

Figure S5. Spherical domain radius, r_A, for gels formulated with two triblock copolymers as a function of copolymer ratio and total copolymer concentration (labeled): $S_{218}EP_{5468}S_{218}$ and $S_{353}EP_{4944}S_{353}$ (a), $S_{353}EP_{4944}S_{353}$ and $S_{161}EP_{2961}S_{161}$ (b), and $S_{218}EP_{5468}S_{218}$ and $S_{161}EP_{2961}S_{161}$ (c). Additionally, intermicelle spacing, l_{AA}, for gels formulated with two triblock copolymers as a function of copolymer ratio and total copolymer concentration (labeled): $S_{218}EP_{5468}S_{218}$ and $S_{353}EP_{4944}S_{353}$ (d), $S_{353}EP_{4944}S_{353}$ and $S_{161}EP_{2961}S_{161}$ (e), and $S_{218}EP_{5468}S_{218}$ and $S_{161}EP_{2961}S_{161}$ (f). Solid lines are a guide to the eye.